IEEE Photonics Journal
An IEEE Photonics Society Publication

Open Access

Wavelength Conversion Efficiency Enhancement in Modal Phase Matched $\chi^{(2)}$ Nonlinear Waveguides

Volume 13, Number 3, June 2021

Dongpeng Kang, ***Member, IEEE***
Weiqi Zhang
Amr S. Helmy, ***Senior Member, IEEE***
Siyuan Yu
Liying Tan
Jing Ma

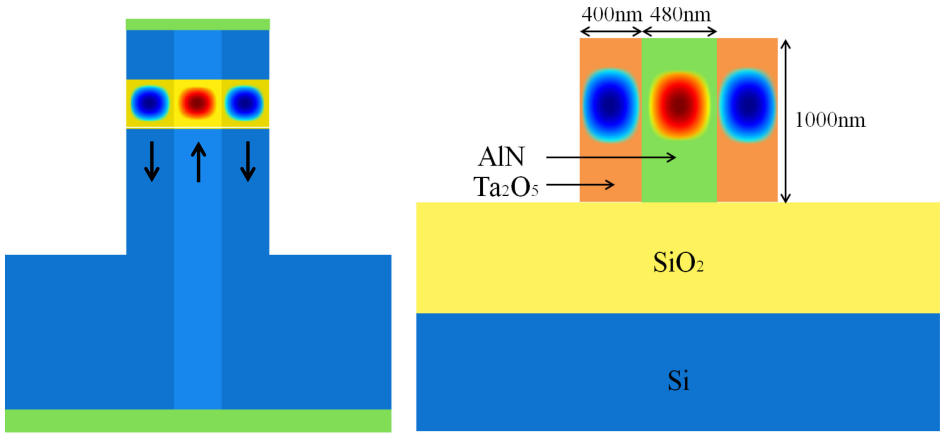

DOI: 10.1109/JPHOT.2021.3087606

Wavelength Conversion Efficiency Enhancement in Modal Phase Matched $\chi^{(2)}$ Nonlinear Waveguides

Dongpeng Kang,[1] ***Member, IEEE***, **Weiqi Zhang**,[1] **Amr S. Helmy**,[2] ***Senior Member, IEEE***, **Siyuan Yu**,[1] **Liying Tan**,[1] **and Jing Ma**[1]

[1]School of Astronautics and National Key Laboratory of Science and Technology on Tunable Laser, Harbin Institute of Technology, Harbin 150001, China
[2]The Edward S. Rogers Department of Electrical and Computer Engineering, Centre for Quantum Information and Quantum Control, University of Toronto, Toronto, ON M5S 3G4, Canada

DOI:10.1109/JPHOT.2021.3087606

Manuscript received April 28, 2021; accepted June 5, 2021. Date of publication June 8, 2021; date of current version June 24, 2021. This work was supported in part by the National Natural Science Foundation of China under Grant 61705053, in part by China Postdoctoral Science Foundation under Grant 2016M600249, and in part by the Heilongjiang Provincial Postdoctoral Science Fundation, Fundamental Research Funds for the Central Universities, and Natural Sciences and Engineering Research Council of Canada. Corresponding authors: Dongpeng Kang and Jing Ma (e-mail: dongpeng.kang@hit.edu.cn; majing@hit.edu.cn).

Abstract: Modal phase matching (MPM) is a widely used phase matching technique in $Al_xGa_{1-x}As$ and other $\chi^{(2)}$ nonlinear waveguides for efficient wavelength conversions. The use of a non-fundamental spatial mode compensates the material dispersion but also reduces the spatial overlap of the three interacting waves and therefore limits the conversion efficiency. In this work, we develop a technique to increase the nonlinear overlap by modifying the material nonlinearity, instead of the traditional method of optimizing the modal field profiles. This could eliminate the limiting factor of low spatial overlap inherent to MPM and significantly enhance the conversion efficiency. Among the design examples provided, this technique could increase the conversion efficiency by a factor of up to ~290 in an $Al_xGa_{1-x}As$ waveguide. We further show that this technique is applicable to all $\chi^{(2)}$ material systems that utilize MPM for wavelength conversion.

Index Terms: Wavelength conversion, second harmonic generation, difference frequency generation, modal phase matching, compound semiconductor, Aluminum Gallium Arsenide.

1. Introduction

Wavelength conversion in nonlinear materials plays an important role in a broad range of classical and quantum optical applications, including optical parametric amplification [1], supercontinuum generation [2], all-optical signal processing [3], sensing [4], photon pair generation [5], [6], and squeezed state generation [7], etc. Compact and efficient wavelength conversion can be achieved in nonlinear waveguides, in which the interacting fields are tightly confined for a long interaction length comparing to their bulk crystal counterparts. Waveguide based wavelength converters also make chip-scale integration with various active and passive components possible, enabling practical devices with new functionalities. In addition, waveguide dispersion provides an additional

tuning knob in certain applications of wavelength conversion such as frequency comb generation [8] and pure heralded single photon generation [9], [10].

Among popular $\chi^{(2)}$ nonlinear materials such as ferroelectrics (mainly lithium niobate), AlN, GaP, etc, compound semiconductor $Al_xGa_{1-x}As$ is uniquely attractive due to one of the highest $\chi^{(2)}$ coefficients ($d_{14}\approx$119 pm/V for GaAs), large transparency window from 0.9 μm to 17 μm, mature fabrication techniques, and perhaps in particular the ability of monolithic integration with active components due to its direct bandgap nature. However, phase matching in $Al_xGa_{1-x}As$ is challenging due to the formidable material dispersion near its bandgap and its non-ferroelectric nature. Several phase matching techniques have been developed for $Al_xGa_{1-x}As$ waveguides, including form-birefringence phase matching using low index AlOx layers [11], [12], quasi-phase matching (QPM) using etch and regrowth process [13]–[15] or quantum-well intermixing (QWI) [16]–[18], modal phase matching (MPM) using either a higher order spatial mode [19], [20] or a mode guided by Bragg reflections [21], [22]. More recently, QPM in suspended whisper-gallering-mode microdisks [23] and snake-shaped curved waveguides [24] have been demonstrated. In addition, high index contrast thin film AlGaAs-on-insulator waveguides enabled by wafer-bonding have shown the capabilities of birefringence phase matching [25] as well as QPM in resonant micro-cavities [26].

While each of the above mentioned techniques shows certain advantages, the most efficient wavelength conversion to date, to the best of our knowledge, in any non-resonant monolithic platform was demonstrated in Bragg reflection waveguides (BRWs) employing MPM [21]. Yet, among all phase matching techniques, MPM in general has the lowest modal field overlap due to the oscillating feature of one of the interacting fields. Although this limiting factor can be alleviated to some extent through epi-structure engineering which reduces the amount of negative electric field in the associated mode [19], [21], further improving the modal overlap, and thus the conversion efficiency, has not been reported in any $Al_xGa_{1-x}As$ waveguide using MPM.

In this work, we develop a technique to improve the conversion efficiency in a MPM waveguide by increasing its nonlinear modal overlap. Instead of attempting to optimize the shape of modal fields, we modify the material nonlinearity according to the sign of the modal electric field involved. Conversion efficiency enhancements are verified through a few design examples. Among them, this technique could improve the conversion efficiency by a factor of over 200 in the best case scenario. In addition, this technique is not limited to $Al_xGa_{1-x}As$ but can also be applied to all $\chi^{(2)}$ material systems which utilize MPM for wavelength conversion.

2. Theory and Method

We consider a generic three-wave mixing process, in which the pump (p) and signal (s) beams are mixed to produce an idler (i). For collinear propagation in the waveguide along the z-axis, the spatial-temporal dependence of the electric field of each interaction mode is given by

$$E_j(x, y, z, t) = A_j(z)E_j(x, y)\exp[-j(\beta_j z - \omega_j t)], \tag{1}$$

where $j \in \{p, s, i\}$, and $A_j(z)$ and $E_j(x, y)$ are the slowly varying amplitude and spatial modal profile, respectively; ω_j is the angular frequency; β_j is the propagation constant given by $\beta_j = 2\pi n_j/\lambda_j$, where n_j and λ_j are the corresponding effective modal index and wavelength respectively.

In the case of continuous wave excitation, we can neglect effects of group velocity mismatch and third-order nonlinearities. The couple-mode equations are given by [27]

$$\frac{dA_p(z)}{dz} = -j\rho_p\xi A_s^* A_i \exp[-j\Delta\beta z] - \frac{\alpha_p}{2}A_p, \tag{2}$$

$$\frac{dA_s(z)}{dz} = -j\rho_s\xi A_p^* A_i \exp[-j\Delta\beta z] - \frac{\alpha_s}{2}A_s, \tag{3}$$

$$\frac{dA_i(z)}{dz} = -j\rho_i\xi A_p A_s \exp[j\Delta\beta z] - \frac{\alpha_i}{2}A_i, \tag{4}$$

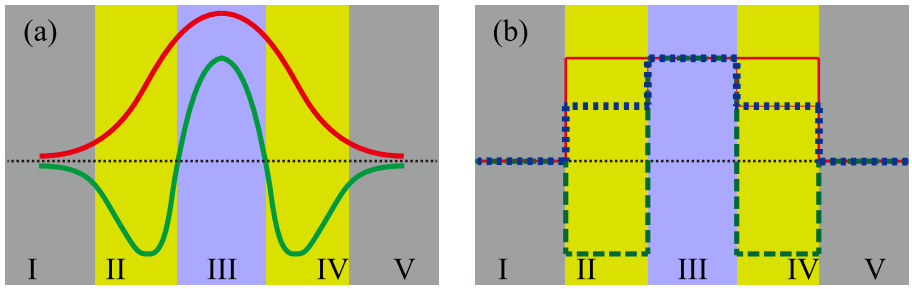

Fig. 1. (a) Schematic of a three-layer slab waveguide using MPM with a fundamental mode (red) and a third order mode (green). The waveguide core consists of regions II, III, and IV, while the claddings are regions I and V. (b) Material nonlinearity distributions for the original waveguide (red solid line) and modified waveguides with negative nonlinearity (green dashed line) and reduced nonlinearity (blue dotted line). The claddings are assumed to have zero nonlinearity.

where α_j is the linear loss coefficient and $\Delta\beta = \beta_i - \beta_s - \beta_p$ is the wave number mismatch. Here we define coefficients ρ_j and the *nonlinear overlap factor* ξ as

$$\rho_j = \left(\frac{8\pi^2}{n_p n_s n_i c\epsilon_0 \lambda_j^2}\right)^{1/2}, \tag{5}$$

$$\xi = \frac{\iint d(x,y)E_p^*(x,y)E_s(x,y)E_i(x,y)\mathrm{d}x\mathrm{d}y}{\left(\iint |E_p^*(x,y)|^2\mathrm{d}x\mathrm{d}y \iint |E_s^*(x,y)|^2\mathrm{d}x\mathrm{d}y \iint |E_i^*(x,y)|^2\mathrm{d}x\mathrm{d}y\right)^{1/2}}, \tag{6}$$

where c and ϵ_0 are the speed of light and vacuum permittivity, respectively, while $d(x,y)$ is the spatial distribution of the effective second order nonlinearity, after taking into account all tensor elements involved. In the case of $\omega_p = \omega_s$, Eqs. (2)–(4) describe a second harmonic generation (SHG) process, otherwise a sum frequency generation (SFG) process. The coupled-mode equations for difference frequency generation (DFG) can be modified accordingly.

In the absence of propagation losses, the normalized conversion efficiency, defined by $\eta = P_i/(P_p P_s L^2)$, is given by

$$\eta = \rho_i^2 |\xi|^2 \,\mathrm{sinc}^2\,(\Delta\beta L/2), \tag{7}$$

where L is the nonlinear waveguide length. According to Eq. (7), the maximum conversion efficiency in a lossless waveguide is uniquely determined by its nonlinear overlap factor given by Eq. (6).

It should be noted that, the nonlinear overlap factor ξ is not determined by the modal overlap of the interacting fields themselves, but instead the overlap of material nonlinearity and the modal fields involved. To illustrate this point, we show schematically in Fig. 1 (a) a slab waveguide using MPM to achieve SHG, where two photons in a fundamental mode are converted to one photon of half the wavelength in a third order mode. Ideally, the two modes need to have the same spatial distribution to obtain the maximum conversion efficiency. However, the third order mode has both positive and negative electric field components, as shown in Fig. 1 (a), which cancel out the contribution of each other in the overlap integral in Eq. (6). This leads to a decreased nonlinear overlap factor and thus severely limits the conversion efficiency of MPM in general.

To reduce this limitation, the conventional technique is to minimize the negative components of the modal field involved in MPM through epi-structure engineering, such as the third order mode in a optimized M-waveguide [19], or the Bragg mode in a BRW [21]. Nevertheless, the nonlinear overlap factors in such cases are still low, due to the unavoidable existence of negative field components. Here we propose an alternative solution which can overcome this limitation. Without even attempting to optimize the field profiles, instead, we modify the spatial distribution of the second order nonlinearity $d(x,y)$ such that it has negative values wherever the high order mode has negative modal components. As such, the negative parts of the modal field will not cancel out the positive parts in the overlap integral in Eq. (6).

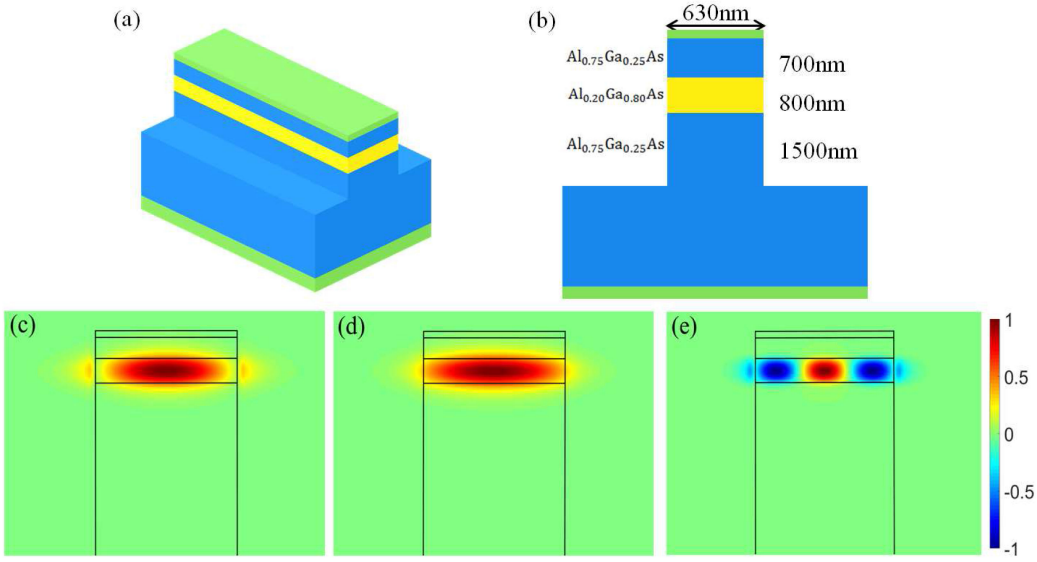

Fig. 2. (a) Schematic of the $Al_xGa_{1-x}As$ ridge waveguide; (b) Waveguide cross-section with a ridge width of 630 nm for MPM; (c)-(e) The electric field profiles of the TE (E_x) and TM (E_y) fundamental modes at 1550 nm and that of the third-order TE_{20} (E_x) mode at 775 nm, respectively.

Taking the structure shown in Fig. 1 (a) for example, the nonlinear overlap factor, and thus the conversion efficiency, can be maximized if the material nonlinearity in regions II and IV has a opposite sign to that of region III, as shown in Fig. 1 (b). This could be achieved by alternating the crystal orientation if the nonlinear coefficient is dependent on it, such as the case of compound semiconductors. If reversing the sign of nonlinearty is not achievable, the conversion efficiency could also be improved by reducing the magnitude of nonlinearty in regions II and IV, or region III, as also shown in Fig. 1 (b).

3. Design Examples

3.1 Reversing the Sign of $d(x, y)$

To illustrate the technique presented above, we first provide an comparative example of $Al_xGa_{1-x}As$ waveguide utilizing MPM, as schematically shown in Fig. 2. The structure is grown on a GaAs [001] substrate with a detailed epi-structure given in Fig. 2(b), and ridge waveguides are patterned along [110] direction. For a ridge width of 0.63 μm in a deeply etched waveguide, type-II phase matching is achieved between the TE_{00} and TM_{00} modes at 1550 nm and the TE_{20} mode at 775 nm, with the modal electric field profiles shown in Figs. 2(c)-(e), respectively. The nonlinear overlap factor, and thus the conversion efficiency is limited the coexistence of both positive and negative electric field components in the second harmonic (SH).

A new design that achieves the maximal conversion efficiency requires the material nonlinearity $d(x, y)$ to be negative wherever the high order mode (TE_{20} in this case) has negative electric field components. In $Al_xGa_{1-x}As$, the effective value of $d(x, y)$ depends on the modal polarizations and the propagation direction. Its dependence on the propagation direction scales as $\cos(2\theta)$, with θ being the angle between propagation direction and the crystalline direction of [110]. As such, the sign of $d(x, y)$ is reversed if the waves propagate along $[\bar{1}10]$. This property has been applied in a variety of QPM techniques, including orientation-patterned QPM (OP-QPM) [15], micro-ring and micro-disks [23], as well as zig-zag [28] and "snake-shaped" waveguides [24]. By utilizing this property, we design a new structure with domain inversion, in which the crystal is rotated 90° in the regions where the TE_{20} mode at SH has negative field components, as shown in Fig. 3(a). Such

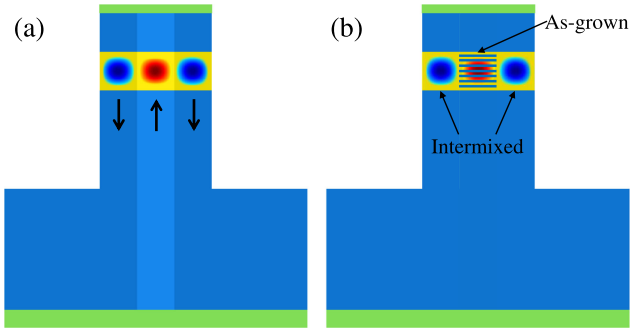

Fig. 3. (a) Schematic of a domain inverted $Al_xGa_{1-x}As$ ridge waveguide superimposed with the electric field profile of the TE_{20} mode at 775 nm, whose positive and negative components reside in domains of orthogonal orientations; (b) Schematics of an $Al_xGa_{1-x}As$ ridge waveguide employing QWI to selectively reduce the magnitude of nonlinearity in regions where the TE_{20} mode at 775 nm has negative field components.

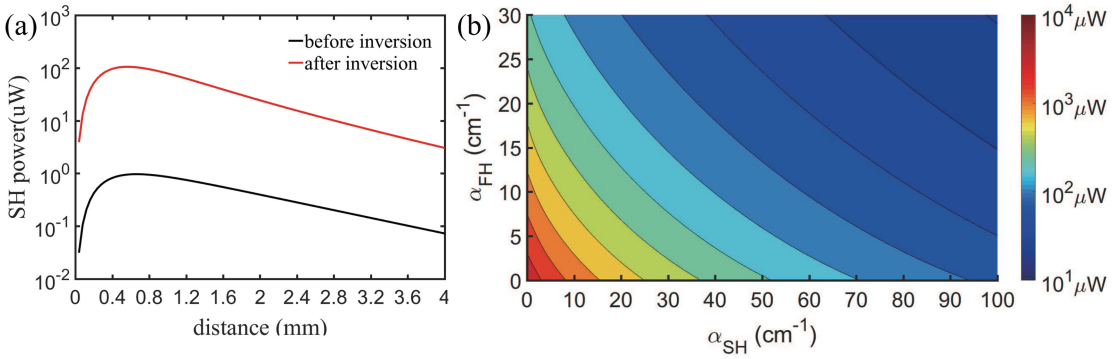

Fig. 4. (a) SH output powers as functions of propagation distance in waveguides without and with domain inversion; (b) Maximal SH power as a function of fundamental frequency and SH propagation losses.

waveguides could be fabricated by similar techniques used by orientation-patterned waveguides, except that the ridges are etched along, rather than perpendicular to the interfaces of alternating domains.

Since the material is optically isotropic, the modal profiles, effective indices and the phase matching condition in the new design are unchanged in the ideal case. With $d(x, y)$ having negative values where the TE_{20} mode field components are also negative, the nonlinear overlap is increased by a factor of 17, leading to an increase of the conversion efficiency by a factor of $\sim$290 if the waveguide is lossless.

In an actual waveguide, the conversion efficiency is also affected by propagation losses. We assumed typical losses of $\alpha_{FH} = 4.2$ cm^{-1} (18.3 dB/cm) for the fundamentals at 1550 nm and $\alpha_{SH} = 73.7$ cm^{-1} (320 dB/cm) for the SH [20], adopted from similar samples in the literatures, and solve the couple-mode equations given by Eqs. (2)–(4) for SHG with an input power of 1 mW in each polarization. The dependence of SH powers on the propagation distance are given by Fig. 4(a) for waveguides without and with domain inversion. Maximal SH powers of 0.97 μ W and 105.1 μW are produced with optimal propagation distances of 0.68 mm and 0.56 mm, respectively, showing an increase of the normalized conversion efficiency η by a factor of $\sim$160, from 5.2×10^3 %W^{-1} cm^{-2} to 8.4×10^5 %W^{-1} cm^{-2}.

In the structure with domain inversion, the losses are likely higher than those in the reference design due to two additional interfaces. Therefore we investigated the dependence of maximal SH power on the losses, as shown in Fig. 4(b). The maximal SH power decreases as the increase

of fundamental and/or SH losses, as expected. However, an enhancement of the conversion efficiency could still be obtained as long as neither of the losses is increased by over 10 folds. As a comparison, the additional losses due to back scattering from hundreds of interfaces between inverted domains can be limited to a few dB/cm in the case of OP-QPM with the state of the art fabrication [14], [15]. This value could be a reasonable expectation for the loss increase in our design.

Notice that fabricating ridge waveguides of such high aspect ratio and precision control is possible but challenging. In the above example, ridges as narrow as of ~200 nm wide are required to be etched in the orientation-patterning process. This fabrication requirement can be eased significantly for longer phase matching wavelengths due to reduced material dispersions. For instance, a similar ridge waveguide can be designed to generate mid-infrared radiation at an output idler wavelength around 7.5 μm in its TE_{00} mode via a DFG process with the input pump at around 1550 nm in its TE_{20} mode and signal at 1950 nm in the TM_{00} mode [29]. The ridge width required for phase matching is increased by a factor of 3.5 to 2.2 μm. With domain inversion, the nonlinear overlap factor and the conversion efficiency are increased by a factor of 11 and 113, respectively, in a lossless waveguide. With representative loss values of 42.6 cm^{-1} (185 dB/cm), 5.4 cm^{-1} (23 dB/cm) and 18.6 cm^{-1} (81 dB/cm) for pump, signal and idler, respectively, the normalized conversion efficiency is increased by a factor of 56 from 0.90 $\%W^{-1}\ cm^{-2}$ to 50.8 $\%W^{-1}\ cm^{-2}$.

3.2 Reducing the Magnitude of $d(x, y)$

In cases that reversing the sign of $d(x, y)$ is impractical, the conversion efficiency could still be improved as long as the magnitude of $d(x, y)$ is reduced in the corresponding regions. In $Al_xGa_{1-x}As$ waveguides, the magnitude of $d(x, y)$ can be reduced by the technique of QWI if a quantum-well superlattice is embedded in the waveguide core [16], [17]. This technique has been commonly used in domain-disordered QPM (DD-QPM), where the nonlinearity is periodically reduced along the direction of propagation. Comparing to OP-QPM, DD-QPM using QWI does not required any etch-and-regrowth fabrication process, and thus the waveguide losses are not considerably increased.

Here we consider QWI being used in previous design examples to reduce the magnitude of $d(x, y)$ instead of reversing its sign by orientation patterning. The superlattice core is selectively intermixed such that the magnitude of $d(x, y)$ is reduced in regions where the TE_{20} mode has negative modal field components, as shown in Fig. 3(b). Assuming that $d(x, y)$ is reduced by a theoretical maximal value of 50 pm/V [30] while the waveguide losses are unchanged, the normalized conversion efficiencies for corresponding SHG and DFG processes are increased by factors of 4 and 9, to $1.9 \times 10^4\ \%W^{-1}\ cm^{-2}$ and $7.8\ \%W^{-1}\ cm^{-2}$, respectively.

The realization of these structures using QWI in quantum confined heterostructures has been reported before by some of the authors. For example, having features on the order of 1 μm has been reported before, and the transition between intermixed and un-intermixed regions is on the sub-micron scale [17]. After intermixing, plasma etching can be used to define the final width of the total waveguide width with an un-intermixed core and two lateral, intermixed layers on either side of that core. Nevertheless, the fabrication requirement can be lowered at a longer phase matching wavelength, where the material dispersion is smaller.

Note that this strategy of improving the nonlinear overlap factor does not only apply for MPM in compound semiconductors but also in all applicable material systems. The reduction of material nonlinearity can also be achieved by incorporating materials with smaller or no nonlinearity in a multi-layer waveguide core. Here we offer an example based on newly developed aluminum nitride (AlN)-on-insulator platform, which has been demonstrated for applications such as electro-optic modulation [31], nonlinear wavelength conversion [32], as well as photon pair generation [33]. MPM between the TM_{00} mode at 1550 nm and the TM_{20} mode at 775 nm in AlN waveguides can be achieved by choosing an appropriate waveguide dimension, similar to previously shown $Al_xGa_{1-x}As$ waveguide designs. The c axis of polycrystalline AlN is perpendicular to the wafer in order to exploit the largest component of AlN's $\chi^{(2)}$ tensor (d_{33}) [31].

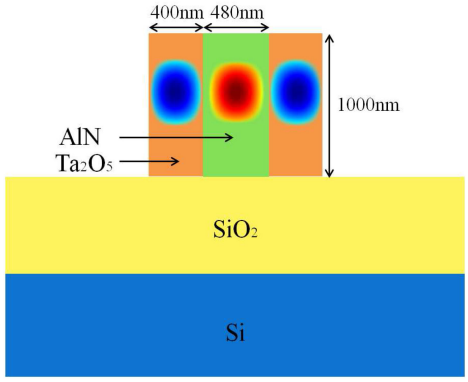

Fig. 5. Schematic of the modified AlN-on-insulator ridge waveguide superimposed with field profile of the TM_{20} mode at 775 nm.

TABLE I

Summary of Normalized Conversion Efficiencies for All Design Examples Provided in Sec. III. Here η_{ref} Represents the Normalized Conversion Efficiency in the Reference Design, While η_{mod} Represents That of the Modified Design Using the Proposed Technique. Waveguide Losses are All Included in the Calculations.

example	frequency conversion process	η_{ref} (%W^{-1}cm^{-2})	η_{mod} (%W^{-1}cm^{-2})	$\eta_{\text{mod}}/\eta_{\text{ref}}$
$Al_xGa_{1-x}As$ inversion	$\omega_{1550}+\omega_{1550}\rightarrow\omega_{775}$	5.2×10^3	8.4×10^5	160
	$\omega_{1550}-\omega_{1950}\rightarrow\omega_{7556}$	0.90	50.8	56
$Al_xGa_{1-x}As$ QWI	$\omega_{1550}+\omega_{1550}\rightarrow\omega_{775}$	5.2×10^3	1.9×10^4	4
	$\omega_{1550}-\omega_{1950}\rightarrow\omega_{7556}$	0.90	7.8	9
AlN	$\omega_{1550}+\omega_{1550}\rightarrow\omega_{775}$	0.11	1.27	12

In the modified design, the AlN ridge is sandwiched by a pair of Ta_2O_5 dielectric such that the positive part of the TM_{20} mode at 775 nm locates in AlN while the negative parts locate in Ta_2O_5, as shown in Fig. 5. The fabrication of these structures can be easily achieved using a two-step lithography process, where initial core ridges are fabricated using lithography and plasma etching. A subsequent process of conformal deposition of the outer regions of the core is carried out. The deposition time and conformal profile of this process can be tuned to suite the required dimensions of the outer layers of the core. Finally, a lithography along with plasma etching process can then follow to achieve the profile and dimensions discussed in this work. Here Ta_2O_5 is chosen because it has an index of refraction close to that of AlN, and it has near-zero second order nonlinearity. This leads to an increase of the nonlinear overlap factor by a factor of ~12 and the SHG efficiency by 144 without waveguide losses. With realistic losses of 2.6 cm^{-1} (11.3 dB/cm) and 86 cm^{-1} (373 dB/cm) for the fundamental and SH [31], the normalized efficiency is increased by a factor of 12 from 0.11 %W^{-1} cm^{-2} to 1.27 %W^{-1} cm^{-2}.

4. Discussion and Conclusion

Design examples provided above demonstrate the effectiveness of the proposed technique. In the best case scenario, we observe up to ~290 folds enhancement in the conversion efficiency assuming the waveguide does not include any losses. With the existence of losses, the conversion efficiency can still be improved significantly. The results are summarized in Table I. It should be emphasized that the technique proposed here applies to $\chi^{(2)}$ nonlinear waveguides of all material systems that adopt MPM in principle, despite it was mainly motivated for compound semiconductors.

The use of specific spatial modes in these designs poses strict constraints on the waveguide width in each etch process. Deviation from the ideal value causes the shift of phase matching wavelength and the decrease of nonlinear overlap. Fabrication of these structures is certainly nontrivial but still practical, as discussed above. After all, techniques including orientation-patterning and QWI have been developed in domain-reversal and domain-suppressed QPM respectively, and high aspect ratio waveguides with low losses and precision etch control have also been achieved [34], [35]. In addition, the use of a higher order mode may first seem intimidating as it often has no easy access. However, waveguide couplers can be implemented to selectively couple light from a neighboring single mode waveguide into the higher order mode, and vice versa, as demonstrated in [32], [33].

Although we use TE_{20} and TM_{20} modes in the design examples, this technique could be applied to MPM waveguides using any other spatial mode provided the material nonlinearity can be modified accordingly. In above designs, material nonlinearities are altered horizontally (parallel to the wafer surface), and horizontal higher order modes (TE_{20} and TM_{20}) are defined lithographically to achieve phase matching. Instead, if material nonlinearities can be modified in the vertical direction (perpendicular to the wafer surface), and the thickness of each layer can be accurately controlled, vertical higher order modes, such as TE_{02} and TM_{02}, can be used. In such cases, requirements on ridge width and etch depth can be significantly relaxed. For instance, in $Al_xGa_{1-x}As$, quantum-well superlattices could be embedded in the epi-stricture of a M-shaped waveguide [19] or a BRW [21], [22], [29] followed by intermixing to reduce the material nonlinearity in certain regions. As for AlN, it can be deposited on a layer of Ta_2O_5 on silica, followed by a cap Ta_2O_5 layer. In this case, the TM_{02} mode is used for the SH, while the ridge width is non-essential. During the preparation of this manuscript, we noticed a recent work based on thin film lithium niobate waveguides which took a strategy similar to this AlN example to increase the conversion efficiency [36].

This technique could be used in conjunction with resonant structures to further enhance the conversion efficiency. For example, the $Al_xGa_{1-x}As$ waveguides given above can be embedded in Fabry-Pérot type cavities, and the AlN waveguides can be lithographically defined as ring resonators [32].

In summary, we have developed a technique to increase the nonlinear overlap factor and therefore the wavelength conversion efficiency in $\chi^{(2)}$ waveguides utilizing MPM. In contrary to the conventional method of optimizing modal field overlap, we modify the material nonlinearity by either reversing the sign or reducing the magnitude in regions which coincide with the negative parts of the high frequency mode. This could eliminate the limiting factor of low nonlinear overlap inherent to MPM and thus fully harness the material nonlinearity for efficient wavelength conversions.

References

[1] Y. Lin, Y. Nabekawa, and K. Midorikawa, "Optical parametric amplification of sub-cycle shortwave infrared pulses," *Nature Commun.*, vol. 11, 2020, Art. no. 3413.

[2] K. Werner *et al.*, "Ultrafast mid-infrared high harmonic and supercontinuum generation with n_2 characterization in zinc selenide," *Opt. Exp.*, vol. 27, no. 3, pp. 2867–2885, Feb. 2019. [Online]. Available: http://www.opticsexpress.org/abstract.cfm?URI=oe-27-3-2867

[3] A. E. Willner, S. Khaleghi, M. R. Chitgarha, and O. F. Yilmaz, "All-optical signal processing," *J. Lightw. Technol.*, vol. 32, no. 4, pp. 660–680, Feb. 2014.

[4] M. L. Weichman, P. B. Changala, J. Ye, Z. Chen, M. Yan, and N. Picqué, "Broadband molecular spectroscopy with optical frequency combs," *J. Mol. Spectrosc.*, vol. 355, pp. 66–78, 2019. [Online]. Available: http://www.sciencedirect.com/science/article/pii/S0022285218302881

[5] J. P. Torres, K. Banaszek, and I. Walmsley, "Chapter 5 - engineering nonlinear optic sources of photonic entanglement," *Ser. Progress Opt.*, E. Wolf, Ed Elsevier, 2011, vol. 56, pp. 227–331, 2011. [Online]. Available: http://www.sciencedirect.com/science/article/pii/B9780444538864000058

[6] L. Caspani *et al.*, "Integrated sources of photon quantum states based on nonlinear optics," *Light: Sci. Appl.*, vol. 6, 2017, Art. no. e17100.

[7] A. Dutt, K. Luke, S. Manipatruni, A. L. Gaeta, P. Nussenzveig, and M. Lipson, "On-chip optical squeezing," *Phys. Rev. Appl.*, vol. 3, Apr. 2015, Art. no. 044005. [Online]. Available: https://link.aps.org/doi/10.1103/PhysRevApplied.3.044005

[8] M. Kues *et al.*, "Quantum optical microcombs," *Nature Photon.*, vol. 13, pp. 170–179, 2019.

[9] D. Kang, A. Pang, Y. Zhao, and A. S. Helmy, "Two-photon quantum state engineering in nonlinear photonic nanowires," *J. Opt. Soc. Amer. B*, vol. 31, no. 7, pp. 1581–1589, Jul. 2014. [Online]. Available: http://josab.osa.org/abstract.cfm?URI=josab-31-7-1581

[10] R. P. Marchildon and A. S. Helmy, "Dispersion-enabled quantum state control in integrated photonics," *Optica*, vol. 3, no. 3, pp. 243–251, Mar. 2016. [Online]. Available: http://www.osapublishing.org/optica/abstract.cfm?URI=optica-3-3-243

[11] L. Scaccabarozzi, M. M. Fejer, Y. Huo, S. Fan, X. Yu, and J. S. Harris, "Enhanced second-harmonic generation in AlGaAs/AlxOy tightly confining waveguides and resonant cavities," *Opt. Lett.*, vol. 31, no. 24, pp. 3626–3628, Dec. 2006. [Online]. Available: http://ol.osa.org/abstract.cfm?URI=ol-31-24-3626

[12] M. Savanier *et al.*, "Nearly-degenerate three-wave mixing at 1.55 μm in oxidized AlGaAs waveguides," *Opt. Exp.*, vol. 19, no. 23, pp. 22 582–22587, Nov. 2011. [Online]. Available: http://www.opticsexpress.org/abstract.cfm?URI=oe-19-23-22582

[13] P. S. Kuo *et al.*, "Optical parametric generation of a mid-infrared continuum in orientation-patterned GaAs," *Opt. Lett.*, vol. 31, no. 1, pp. 71–73, Jan. 2006. [Online]. Available: http://ol.osa.org/abstract.cfm?URI=ol-31-1-71

[14] X. Yu, L. Scaccabarozzi, A. C. Lin, M. M. Fejer, and J. S. Harris, "Growth of GaAs with orientation-patterned structures for nonlinear optics," *J. Cryst. Growth*, vol. 301–302, pp. 163–167, 2007. [Online]. Available: http://www.sciencedirect.com/science/article/pii/S0022024806014345

[15] K. Fedorova, A. McRobbie, G. Sokolovskii, P. Schunemann, and E. Rafailov, "Second harmonic generation in a low-loss orientation-patterned GaAs waveguide," *Opt. Exp.*, vol. 21, no. 14, pp. 16424–16430, 2013.

[16] A. S. Helmy *et al.*, "Quasi phase matching in GaAs-AlAs superlattice waveguides through bandgap tuning by use of quantum-well intermixing," *Opt. Lett.*, vol. 25, no. 18, pp. 1370–1372, Sep. 2000. [Online]. Available: http://ol.osa.org/abstract.cfm?URI=ol-25-18-1370

[17] A. S. Helmy, A. C. Bryce, D. C. Hutchings, J. S. Aitchison, and J. H. Marsh, "Band gap gratings using quantum well intermixing for quasi-phase-matching," *J. Appl. Phys.*, vol. 100, no. 12, 2006, Art. no. 123107. [Online]. Available: https://doi.org/10.1063/1.2402034

[18] P. Sarrafi *et al.*, "Continuous-wave quasi-phase-matched waveguide correlated photon pair source on a III-V chip," *Appl. Phys. Lett.*, vol. 103, no. 25, 2013, Art. no. 251115.

[19] S. Ducci, L. Lanco, V. Berger, A. D. Rossi, V. Ortiz, and M. Calligaro, "Continuous-wave second-harmonic generation in modal phase matched semiconductor waveguides," *Appl. Phys. Lett.*, vol. 84, no. 16, pp. 2974–2976, 2004. [Online]. Available: http://link.aip.org/link/?APL/84/2974/1

[20] D. Duchesne *et al.*, "Second harmonic generation in AlGaAs photonic wires using low power continuous wave light," *Opt. Exp.*, vol. 19, no. 13, pp. 12408–12417, Jun. 2011. [Online]. Available: http://www.opticsexpress.org/abstract.cfm?URI=oe-19-13-12408

[21] P. Abolghasem, J. Han, B. J. Bijlani, A. Arjmand, and A. S. Helmy, "Highly efficient second-harmonic generation in monolithic matching layer enhanced $Al_xGa_{1-x}As$ waveguides," *IEEE Photon. Technol. Lett.*, vol. 21, no. 19, pp. 1462–1464, Oct. 2009.

[22] P. Abolghasem, J.-B. Han, D. Kang, B. J. Bijlani, and A. S. Helmy, "Monolithic photonics using second-order optical nonlinearities in multilayer-core Bragg reflection waveguides," *IEEE J. Sel. Topics Quantum Electron*, vol. 18, no. 2, pp. 812–825, Mar./Apr. 2012.

[23] P. S. Kuo, J. Bravo-Abad, and G. S. Solomon, "Second-harmonic generation using quasi-phasematching in a GaAs whispering-gallery-mode microcavity," *Nature Commun.*, vol. 5, 2014, Art. no. 3109.

[24] N. Morais *et al.*, "Directionally induced quasi-phase matching in homogeneous AlGaAs waveguides," *Opt. Lett.*, vol. 42, no. 21, pp. 4287–4290, Nov. 2017. [Online]. Available: http://ol.osa.org/abstract.cfm?URI=ol-42-21-4287

[25] S. May, M. Kues, M. Clerici, and M. Sorel, "Second-harmonic generation in AlGaAs-on-insulator waveguides," *Opt. Lett.*, vol. 44, no. 6, pp. 1339–1342, Mar. 2019. [Online]. Available: http://ol.osa.org/abstract.cfm?URI=ol-44-6-1339

[26] L. Chang *et al.*, "Strong frequency conversion in heterogeneously integrated GaAs resonators," *APL Photon.*, vol. 4, no. 3, 2019, Art. no. 0 36103. [Online]. Available: https://doi.org/10.1063/1.5065533

[27] T. Suhara and M. Fujimura, *Waveguide Nonlinear-Optic Devices*. Berlin, Germany: Springer, 2003.

[28] R. T. Horn and G. Weihs, "Directional quasi-phase matching in curved waveguides," 2010, *arXiv:1008.2190*.

[29] D. F. Logan, M. Giguere, A. Villeneuve, and A. S. Helmy, "Widely tunable mid-infrared generation via frequency conversion in semiconductor waveguides," *Opt. Lett.*, vol. 38, no. 21, pp. 4457–4460, Nov. 2013. [Online]. Available: http://ol.osa.org/abstract.cfm?URI=ol-38-21-4457

[30] D. C. Hutchings, "Theory of ultrafast nonlinear refraction in semiconductor superlattices," *IEEE J. Sel. Topics Quantum Electron.*, vol. 10, no. 5, pp. 1124–1132, Sep. 2004.

[31] C. Xiong, W. H. P. Pernice, and H. X. Tang, "Low-loss, silicon integrated, aluminum nitride photonic circuits and their use for electro-optic signal processing," *Nano Lett.*, vol. 12, no. 7, pp. 3562–3568, 2012. [Online]. Available: https://doi.org/10.1021/nl3011885

[32] X. Guo, C.-L. Zou, and H. X. Tang, "Second-harmonic generation in aluminum nitride microrings with 2500%/W conversion efficiency," *Optica*, vol. 3, no. 10, pp. 1126–1131, Oct. 2016.

[33] X. Guo, C.-L. Zou, C. Schuck, H. Jung, and H. X. Tang, "Parametric down-conversion photon-pair source on a nanophotonic chip," *Light: Sci. Appl.*, vol. 6, May 2017, Art. no. e16249.

[34] G. A. Porkolab, P. Apiratikul, B. Wang, S. H. Guo, and C. J. K. Richardson, "Low propagation loss AlGaAs waveguides fabricated with plasma-assisted photoresist reflow," *Opt. Exp.*, vol. 22, no. 7, pp. 7733–7743, Apr. 2014. [Online]. Available: http://www.opticsexpress.org/abstract.cfm?URI=oe-22-7-7733

[35] Z. Liao and J. S. Aitchison, "Precision etching for multi-level AlGaAs waveguides," *Opt. Mater. Exp.*, vol. 7, no. 3, pp. 895–903, Mar. 2017. [Online]. Available: http://www.osapublishing.org/ome/abstract.cfm?URI=ome-7-3-895

[36] R. Luo, Y. He, H. Liang, M. Li, and Q. Lin, "Semi-nonlinear nanophotonic waveguides for highly efficient second-harmonic generation," *Laser Photon. Rev.*, vol. 13, no. 3, 2019, Art. no. 1800288, 2019. [Online]. Available: https://onlinelibrary.wiley.com/doi/abs/10.1002/lpor.201800288